The Impact of Improved Weak Interaction Physics in Core-Collapse Supernova Simulations

O. E. Bronson Messer[1,2,3], Matthias Liebendörfer[1,2], W. Raphael Hix[1,2,3], Anthony Mezzacappa[2], and Stephen W. Bruenn[4]

[1] University of Tennessee, Knoxville TN 37996, USA
[2] Oak Ridge National Laboratory, Oak Ridge TN 37831, USA
[3] Joint Institute for Heavy Ion Research, Oak Ridge TN 37831, USA
[4] Florida Atlantic University, Boca Raton FL 33432, USA

Abstract. Recent core-collapse supernova simulations incorporating Boltzmann neutrino transport have highlighted the need for an improved set of "standard" microphysics to be employed in such simulations. Improved electron capture rates on nuclei during core collapse, the inclusion of nucleon-nucleon bremsstrahlung, and the effects of weak magnetism and the strangeness content of the nucleon are three examples. We discuss the initial implementation of these improvements in fully self-consistent radiation hydrodynamic core-collapse supernova simulations incorporating Boltzmann neutrino transport.

1 Motivation

The most recent generation of core-collapse supernova simulations employing state-of-the-art neutrino transport [19][16][9] make use of a set of weak interaction physics primarily due to [1]. The failure of these simulations to produce explosions in spherical symmetry suggests an update of the microphysical inputs is necessary to fully determine the sensitivity of the simulations to the description of the neutrino-matter interactions.

2 Improved Electron Capture Rates During Core Collapse

Heger et al. [5](HLMPW01) have repeated the evolution calculations of Woosley & Weaver [21](WW95) for initial progenitor masses of $15\,M_\odot$, $25\,M_\odot$, and $40 M_\odot$, replacing the weak interaction rates for electron and positron captures and β^- and β^+ decays. The WW95 models used the electron capture rates of [2](FFN) and older sets of beta decay rates [12][4]. HLMPW01 have updated both with a new set of shell model weak interaction rates for electron capture, positron capture, and β^- and β^+ decays [8][18]. The most noticeable effect of these changes is a marked increase in the electron fraction (Y_e) throughout the iron core before collapse. Because the final size of the homologous core, and therefore the shock formation radius, is proportional to the square of the trapped lepton fraction (${Y_l}^2$) at core bounce [22], the persistence of these initial differences in Y_e throughout collapse might have a discernible effect on the shock energetics.

In an initial attempt to determine the influence of these improved rates on iron core collapse, we have performed full radiation hydrodynamic collapse simulations using the neutrino radiation hydrodynamics code AGILE-BOLTZTRAN [14][17][10][11].

We observe no difference in initial shock formation position between the two sets of progenitor models when our set of standard physics is used [13]. In these cases, capture rates on nuclei are quickly shut off when $A > 65$, and the capture rate on free nucleons dominates. The steep dependence of the free proton fraction on changes in the electron fraction assures convergence to the same Y_e profile inside the homologous core. We have also performed simulations in which the electron capture rate on nuclei was turned off as well as simulations in which the capture rate on free nucleons was increased by a factor of 10. Neither parameterization had any discernible effect on the shock formation radius.

In an attempt to investigate the impact of including the updated electron capture rates during core collapse we have also performed collapse simulations with the HLMPW01 15 $M_\odot$ core with a parameterized form of our usual electron capture rates. We write the neutrino emissivity from nuclei as [1][15]:

$$j_{nuc} = \frac{2}{7}\frac{(2\pi)^4 G_F^2 g_A^2}{\pi h^4 c^4}\frac{\rho X_H}{m_B A} N_p(Z) N_h(N)(E+Q)^2 \left[1-(\frac{M_e}{E+Q})^2\right]^{1/2} F_e(E+Q), \quad (1)$$

where

$$N_p(Z) = \begin{cases} 0 & Z < 20 \\ Z-20 & 20 < Z < 28 \\ 8 & Z > 28 \end{cases} \quad N_h(N) = \begin{cases} 6 & N < 34 \\ 40-N & 34 < N < 40 \\ 0 & N > 40. \end{cases} \quad (2)$$

To parameterize this rate we replace the product $N_p(Z)N_h(N)$ with a constant (0.1, 1, 10, or 100). This parameterization has a significant effect on the formation of the bounce shock. Setting the capture parameter equal to 10 moves the shock formation point inward more than 0.1 $M_\odot$ (0.64 $M_\odot$ versus 0.52 $M_\odot$). The most important feature of the parameterization is the persistence of captures on nuclei throughout collapse. The precise value of the parameter is of secondary importance. The fundamentally different behavior of the parametrized rate as compared to the standard rate is shown in Figure 1.

3 Nucleon-Nucleon Bremsstrahlung

It has recently been shown that nucleon-nucleon bremsstrahlung can be the dominant production mechanism for μ and τ neutrinos and antineutrinos in dense regions of the protoneutron star [3][20]. We have included this process in recent test simulations of core collapse and shock breakout using AGILE-BOLTZTRAN (with reduced angular resolution). The impact on the $\nu_{\mu,\tau}$ luminosity is shown in Figure 2. During collapse, the bremsstrahlung process leads to markedly increased production, as the only other production mechanism, electron-positron pair annihilation, is essentially inoperative. After shock breakout the average neutrino energy is reduced by the inclusion of bremsstrahlung (≈10% throughout most of the core), but the increased flux induced by the softened spectra more than compensates for this reduction, yielding a slightly higher luminosity (≈8% above the shock).

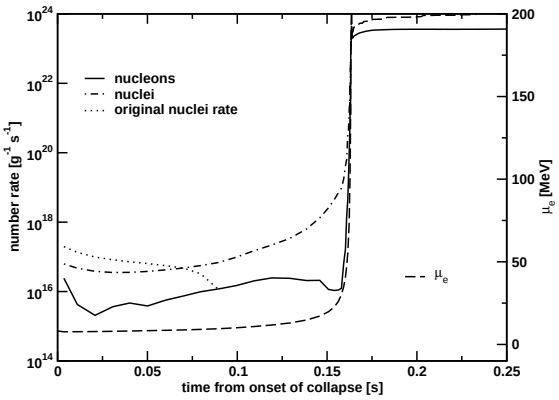

Fig. 1. The number rate of electron captures during core collapse as a function of time. The electron chemical potential is also shown

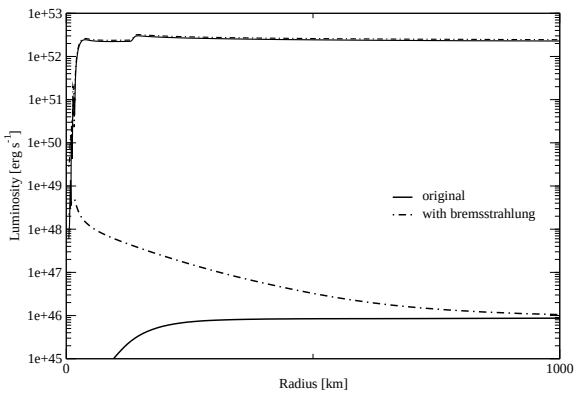

Fig. 2. $\nu_{\mu,\tau}$ luminosities for test runs with and without incorporation of nucleon-nucleon bremsstrahlung. The lower set of curves corresponds to a central density of 6.470×10^{13} g/cm^3, roughly 2 ms before core bounce. The upper curves are just after shock breakout

4 Weak Magnetism

Horowitz [6] gives a simple prescription for the inclusion of weak magnetism effects in neutrino transport calculations. Figure 3 compares neutrino luminosities at 1000 km for simulations incorporating the corrections of [6] for weak magnetism and corrections for the strangeness content of the nucleon [7] to results using our standard set of microphysics. Antineutrino luminosities are most affected, being ≈10% higher when both weak magnetism and strangeness corrections are included. Weak magnetism effects alone produce a ≈6-7% enhancement. Neutrino luminosities behave in much the same way, but the maximum change in luminosity for each flavor is only about half that for the antineutrinos (≈5%).

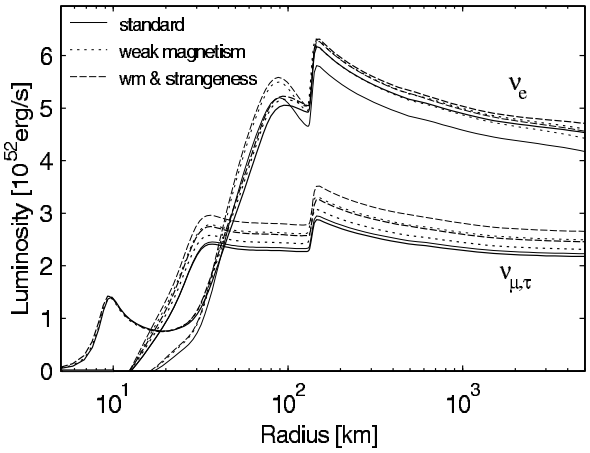

Fig. 3. Neutrino (*heavy lines*) and anitneutrino (*thinner lines*) luminosities at 100 ms post-bounce with standard opacities, including weak magnetism effects, and including both weak magnetism effects and the effect of the strangeness content of the nucleon

5 Acknowledgements

We acknowledge support from the U.S. Department of Energy Scientific Discovery through Advanced Computing Program, the Joint Institue for Heavy Ion Research, the National Science Foundation under contract AST-987713, and NASA under contract NAG5-3903. Oak Ridge National Laboratory is managed by UT-Battelle, LLC, for the U.S. Department of Energy under contract DE-AC05-00OR22725. This research used resources of the National Energy Research Scientific Computing Center, which is supported by the Office of Science of the U.S. Department of Energy under Contract No. DE-AC03-76SF00098.

References

1. S. W. Bruenn: ApJS **58**, 771 (1985)
2. G. M. Fuller, W. A. Fowler, M. J. Newman: ApJS **42**, 447 (1980)
3. S. Hannestad, G. Raffelt: ApJ **507**, 339 (1998)
4. C. J. Hansen: Neutrino Emission from Dense Stellar Interiors. PhD Thesis, Yale University, New Haven (1966)
5. A. Heger, K. Langanke, G. Martínez-Pinedo, S.E. Woosley: Phys. Rev. Lett. **86**, 1678 (2001)
6. C. Horowitz: Phys. Rev. D **65**, 043001 (2002)
7. E. Kolbe, K. Langanke, S. Krewald, F.-K. Thielemann: ApJL **401**, L89, (1992)
8. K. Langanke, G. Martinez-Pinedo: Nucl. Phys. A. **673**, 481 (2000)
9. M. Liebendörfer, A. Mezzacappa, F.-K. Thielemann, O. E. B. Messer, R. W. Hix, S. W. Bruenn: Phys. Rev. D **63**, 103004, (2001)
10. M. Liebendörfer, S. Rosswog, F.-K. Thielemann: ApJS **141**, 229 (2002)
11. M. Liebendörfer, O. E. B. Messer, A. Mezzacappa, S. W. Bruenn, C. Y. Cardall, F.-K. Thielemann: ApJS, submitted (2002)
12. T. J. Mazurek: Thermonuclear Supernova in Binary Helium Dwarfs. PhD thesis, Yeshiva University, New York (1973)
13. O. E. B. Messer, W. R. Hix, M. Liebendörfer, A. Mezzacappa: in preparation
14. A. Mezzacappa, S. W. Bruenn: ApJ **405**, 637 (1993)
15. A. Mezzacappa, S. W. Bruenn: ApJ **405**, 669 (1993)
16. A. Mezzacappa, M. Liebendörfer, O. E. B. Messer, R. W. Hix, F.-K. Thielemann, S. W. Bruenn: Phys. Rev. Lett. **86**, 1935 (2001)
17. A. Mezzacappa, O. E. B. Messer: J. Comp. and App. Mathematics **109**, 281 (1999)
18. T. Oda, M. Hino, K. Muto, M. Takahara, K. Sato: Atomic Data & Nucl. Data Tables **56**, 231 (1994)
19. M. Rampp, H.-T. Janka: ApJL **539**, L33 (2000)
20. T. A. Thompson, A. Burrows, J. E. Horvath: Phys. Rev. C **62**, 035802 (2000)
21. S. E. Woosley, T. A. Weaver: ApJS **101**, 181 (1995)
22. A. Yahil: ApJ **265**, 1047 (1983)